

Transient vibration of shafting in coupled hydraulic-mechanical-electrical-structural system for hydropower station during start-up process

Jinjian Zhang^a, Zhenyue Ma^a, Xueni Wang^b, Qianqian Wu^c, Leike Zhang^{b,*}

^a School of Hydraulic Engineering, Faculty of Infrastructure Engineering, Dalian University of Technology, Dalian 116023, China

^b College of Water Resources Science and Engineering, Taiyuan University of Technology, Taiyuan 030024, China

^c Civil Engineering Institute, Sanjiang University, Nanjing 210012, China

ARTICLE INFO

Keywords:

Coupled hydraulic-mechanical-electrical-structural system
Transient process
Static and dynamic eccentricity
Electromagnetic excitation
Vibration property

ABSTRACT

The operating parameters of hydroelectric generating system vary constantly in the course of transition, meanwhile, the coupled correlations among hydraulic, mechanical, electrical and structural subsystems are convoluted, which makes the vibration of shafting system prominent, as well as affects the safe and stable operation for hydropower station. In this paper, a coupled hydraulic-mechanical-electrical-structural model for hydroelectric generating system is proposed, while the start-up transient process is incorporated into the investigation system, and the dynamic response from shafting system at different stages attached to start-up process is scrutinized numerically, making allowance for the effect of unbalanced magnetic pull with static and dynamic eccentricity. The kinetic property of structure over the start-up process is illuminated, by means of the comparison with motion trait for system under steady-state operating condition. The results indicate that the dynamic feature of rotor and runner is significantly contrasting in different stages affiliated to the start-up scenario, especially for the voltage building-up subdivision. In addition, the response peculiarity from rotor covering the trajectory, vibration amplitude and frequency components, etc., is markedly altered, due to the participation of static, dynamic eccentricity as well as the matching variation on electromagnetic excitation. The trajectory of rotor evolves from a regular circle to a butterfly-shaped curve, and the associated transient displacement intensifies immensely, besides, the 2x frequency component emerges and corresponding dominant role gradually strengthens, accompanied by a developmental amplitude of 1x frequency in spectrum diagram. Relevant research results can provide profitable reference for the analysis of dynamic characteristic on hydropower station through transient conditions.

1. Introduction

According to *World Energy Blueprint: World Energy Development Report (2022)* [1], renewable energy will be primary fountainhead of the growth in electricity supply in the future, and account for more than 32% on the total global electricity supply by 2024. As the cornerstone of energy transformation, hydropower is a crucial support to promote the scaled development of new energy sources, such

* Corresponding author at: College of Water Resources Science and Engineering, Taiyuan University of Technology, Taiyuan 030024, Shanxi, China.

E-mail address: lkzhang@hotmail.com (L. Zhang).

Nomenclature

A	Area of penstock
a	Velocity of water hammer wave
b_p	Permanent droop
b_t	Temporary droop
C_w, C_p, C_n	The coefficients associated with Q, H and geometry of penstock in previous time step
c_b	Clearance of bearing
C_f	Frequency command
c_i	Damping coefficients, $i = 1, 2, 3, 4, 5$
c_r	Air gap length of rotor
CSST	The conditions of setting surge tanks
D	Cross section diameter of penstock
D_1	Nominal diameter of turbine
D_0	Damping factor
E'_q	Transient electromotive force (EMF) of q -axis
e_1, e_3	Mass eccentricity of rotor and runner
E_{fd}	Imaginary open-circuit EMF
E_q	No-load terminal EMF
f	Drag coefficient along the path
F_1	Synthetic magnetomotive force amplitude of air gap
f_x, f_y	X- and y - components of nonlinear oil film force
F_x, F_y	X- and y - components of nonlinear sealing force
$F_{x,rub}, F_{y,rub}$	X- and y - components of rub-impact force
g	Gravity acceleration
H	Head of penstock
H_1	The upstream head
HGS	Hydroelectric generating system
HMEs	Coupled hydraulic-mechanical-electrical system
HMESS	Coupled hydraulic-mechanical-electrical-structural system
H_{np}	The net turbine head
H_p	The turbine inlet head
H_{t1}	The difference in height from draft tube to base line
HTPC	Hydraulic turbine performance curves
I, I_d, I_q	Generator current and corresponding d - and q - components, respectively
I_f	Excitation current
J_{p1}, J_{p2}	Moment of inertia for rotor and runner
K	Integrated amplification factor
k_1, k_2, k_3	Stiffness of upper, lower and water guide bearing
K_p, K_I, K_D	The proportional, integral and differential gains of governor, respectively
k_t	Torsional stiffness
L	Length of rotor
L_p	Height of pad
M_{rub}	The frictional moment
M_{ump}	The electromagnetic torque
m_1, m_2, m_3	Mass of rotor, journal and runner
MOC	The method of characteristic
M_b, M_e	The instantaneous rotational torque of turbine and generator, respectively
P_0, P_b, P_e	The rated, mechanical and electromagnetic power of generator, respectively
p	Number of magnetic poles of generator rotor
Q	Discharge of penstock
R	Radius of rotor
R_a	Radius of shaft
R_b	Radius of journal
RBF	The radial basis function
R_i	Inner radius of pad
R_o	Outer radius of pad
SDE	Static and dynamic eccentricity
T'_{do}	The open-circuit transient time constant of d -axis
T_e	Time constant of excitation

as wind and photovoltaic power, as well as build a clean, low-carbon and efficient energy system and new type power structure [2]. The vigorous progression of hydropower is an effective and efficient measure to cope with the current ascent of energy demand, the optimization of energy structure, the energy conservation and emission reduction, also the guarantee of security and stability for power system [3].

As the premier role in regulating tasks for power system consisting of peak load regulation, frequency modulation and phase modulation, hydropower station undergoes the alteration of transient operating conditions frequently referring to start-up, load increase, load rejection and shut-down, on account of high-proportioned penetrations of wind power, photovoltaic power and other renewable energy on power grid and the peak-valley differences of power loads. According to statistics, conventional hydropower station experiences transient process 0.22~0.25 times/hour averagely, while the comparative index of pumped storage power station even reaches several times/hour [4]. The operating uncertainty factors of hydropower station intensify significantly owing to the frequent switchover in operational states, which may affect normal operation of unit, even cause serious accidents. For instance, intense vibration and oscillation occurred in Tianhuangping hydropower station (China) during shut-down, load increase, load rejection, as well as conversion between pumping phase and pumping condition [5]. The instability failure of rotor pole coil happened in Guangdong Huizhou pumped storage power station (China) in the course of grid-connected process, resulting in an explosion of unit [6]. The broken shaft in a Romanian power station was closely related to the frequent start-ups and shut-downs of unit [7]. In 2009, a lifting accident of unit occurred at the Sayano-Shushenskaya hydropower station (Russia) due to the immoderate vibration of unit #2, when passing through a non-recommended operating condition, giving rise to a removal of head cover, the explosion of transformer, the shutdown of power station, the leakage of oil and extensive pollution in Yenisei River [8]. From the above examples, apparently abnormal vibrations of hydropower unit and the resulting accidents mostly occur in the switching process of different working conditions, i.e. the transient scenario, which is usually recognized as an ephemeral moment, and the relevant effect on vibration of unit as well as plant structure is evanescent. Nonetheless, a key fact needed to be stressed is that, despite the short duration of transition process, the vibration amplitude of unit with various external excitation in course of transient process can reach several times or even more of that, when the system is operated stably [9]. Hence, the structural reliability and operational stability of hydropower unit during transient process, are constituted the keys to guarantee the safe and stable operation of hydroelectric generating system (HGS).

The research of transition process for HGS involves hydraulic, mechanical, electrical and structural aspects, which belongs to the typical analysis category of coupled hydraulic-mechanical-electrical-structural system (HMESS). Initially, a third-order model of generator combined with the hydraulic turbine regulation system model in grid-connected operation condition, was proposed by Shen

T_m	Water turbine inertia time constant
T_n	Accelerating time constant
T_w	Water inertia time constant
T_y	Servomotor response time constant
T_{yB}	Reaction time constant of auxiliary servomotor
U_G, U_{Gd}, U_{Gq}	The stator terminal voltage and corresponding d - and q - components, severally
U_L	Load voltage of system
UMP	The unbalanced magnetic pull
x	Input (deviation ratio of rotating speed) variable
X'_d	Transient reactance of d -component
X_d, X_q	Synchronous reactance of d - and q - component
y	Output (servomotor stroke) variable
α	Included angle between air gap position and x -axis
α_1	The angle between pressure pipe axis and horizontal plane
γ	Rotation angle of rotor center
δ	Power angle
δ_0	Average air gap length
δ_s, δ_d	Static and dynamic eccentricity of air gap
Δt	The time step
Δx	The space step
θ_1, θ_2	Torsional angle of rotor and runner
θ_m	Mechanical rotation angle
Λ_0	Constant component of air gap permeance
Λ_s, Λ_d	Magnetic conductivity components attracted by dynamic and static eccentricity
μ_0	Air permeance
φ	Rotation angle of mass center surrounding the geometric center
φ_0	Initial rotating phase
φ_1, φ_2	Rotation angle of rotor and runner
ω	Rotational speed
ω_e	The electrical angular velocity of generator rotor
ω_{es}	Synchronous electrical speed
ω_m	Mechanical angular velocity

et al. [10] in 1989, which opened the research on transient process of the coupled hydraulic-mechanical-electrical system (HMEs) for HGS. On the basis of ideal model, the IEEE group tendered linear and nonlinear models of hydraulic turbines in 1992, taking into consideration nonlinear factors of turbine and interrelated damping effect, friction loss and no-load loss [11]. Subsequently, a nonlinear model for dynamic studies of hydro turbines was put forward by Jaeger et al. [12]. Cheng et al. [13] comprehensively inquired the interconnections of different subsystems in transition process for HMEs. From the perspective of theoretical derivation, a transient analysis method for solving the HMEs model with a long tunnel surge tank was proposed by Zhou et al. [14]. Through the establishment of pumped storage unit group model, Zeng et al. [15] explored transformation law of high water hammer caused by the mutation in individual machine load. The conditions of setting surge tanks (CSST) were summarized and analyzed by Bao et al. [16], moreover, a comprehensive differentiation of CSST under different circumstances was presented. Liu et al. [17] developed a model of grid-connected hydropower station with a surge tank, the coupled dynamic characteristic of system and the connected mechanism among subsystems were revealed. Li et al. [18] provided a new method for the studies on transition process of HMEs, according to the research on transient characteristic for HGS in a sudden load increasing condition, on the basis of Hamilton's principle. Afterwards, Xu et al. [19,20] applied the Hamilton's principle to further develop a mathematical model of transient process for HGS and carried out related kinetic analysis, moreover, the influence of parametric uncertainty upon dynamic trait of system was uncovered. Hou et al. [21] researched the optimal successive start-up strategy of two hydraulic coupling pumped storage units (PSUS), based on a successive start-up model of PSPS, a novel optimization scheme multi-objective for two PSUS with different parameters was put forward. Lei et al. [22] studied the start-up optimization strategies of hydroelectric generating system, proposed a mathematical model of HGS describing the complex hydraulic coupling relationship, between the penstock, the turbine, the governor as well as the generator, and the effect of successive start-up time interval and the pipe structure on the water head and the rotational speed of HGS was explained, the research results provided a theoretical guidance for the selection of optimal start-up strategy under the circumstance of symmetric and asymmetric HGS branch pipe structures. Generalized Hamiltonian dynamic models for the internal shafting system, the external turbine regulating system, and the coupled internal and external system of HGS were established by Wang et al. [23], and the dynamic characteristic and stability of system were revealed from the energy perspective. Taking a shafting system of hydraulic generating set as the investigation target, the transient attribute of shafting was studied by Zeng et al. [24], utilizing a generalized Hamiltonian model with additional input terms, contributing a reference for the simulation of shafting system with multiple vibration sources. By means of lumped parameter method, a mathematical model of shafting system for hydraulic generating set was established by Guo et al. [25], and the vibration feature of generator rotor and turbine runner in load rejection circumstance was exposed. Considering the coupling influence of turbine regulating system and shafting system for HGS, taking a unbalanced hydraulic force model as the entry point, Li et al. [26] created a unified coupled model of turbine regulating system and shafting system, closely associating hydraulic section and electromechanical section, on this basis, the sway of leading operational parameters on vibration feature of unit was disclosed. On these grounds, Guo et al. [27] investigated the effect of different parameters over the vibration rules of unit when system undergoes transient process. Based on the vision of exploring vibration mechanism of unit in HMEs, the analysis models for the fixed guide vane flow-induced excitation, the coupling vibration characteristic of electromechanical system and the simulation model of flow field in transition process about pumping unit were established by Zhou et al. [28], and the ground of vibration, distribution law and evolution mechanism of flow and electromagnetic fields were dissected. Taking the coupling structure of hydraulic generating set and power-house as the research target, combined with the secondary development function of ANSYS, Wu et al. [29] established a transient vibration model of coupled unit-plant structure under the impression of hydraulic-mechanical-electrical factors for the first time, and proposed a research method for dynamic attribute of unit-plant structure during transient process, discussing the influence of transition process on unit and plant structure, successfully, the hydraulic-mechanical-electrical transient process was connected with unit-plant structure. On top of that, Zhang et al. [30] deduced a mathematical expression of hydraulic excitation induced by draft tube vortex under different load conditions, and the sudden load increasing transient process was incorporated into the investigation system of unit-plant structure, providing a reasonable and reliable analysis model and method for dynamic response exploration, stability investigation, as well as fault diagnosis of hydraulic generating set and hydropower plant structure.

In light of the above discussions, the researches on transition process of HGS have evolved from single combinations of hydraulic-mechanical, mechanical-electrical and hydraulic-electrical to complex coupled hydraulic-mechanical-electrical system, as well as incorporated hydraulic generating unit and hydropower plant structure for the achievement of close connection between the hydraulic-mechanical-electrical transient process and unit-plant structure, and relevant products are plentiful and substantial [10–30]. However, these studies aforesaid were mainly focused on the blanket transition processes of start-up, shut-down, grid connection, load increase, load decrease and load rejection in HGS, and the compositions and modification of various stages throughout transient conditions, as well as the effect of resulting fluctuation from hydraulic, mechanical and electrical parameters on dynamic trait of system were discussed deficiently. The start-up process, for instance, includes stages such as speed ramp-up, speed control and voltage building-up process, and multitudinous parameters involving speed, flow, guide vane opening, head, torque and excitation current, are fluctuating over the period. As the essential element of voltage building-up process, excitation current and associated electromagnetic excitation are core components concerning the start-up operating performances of unit. The unbalanced magnetic pull (UMP) is the primary electromagnetic excitation of hydraulic generating set, in addition to excitation current, UMP is also related to the air gap eccentricity. For hydro generator, the air gap eccentricity between stator and rotor can be divided into static eccentricity, dynamic eccentricity and compound eccentricity. The effect of static eccentricity was principally considered in previous reports, while discussions on the impression of dynamic eccentricity and compound eccentricity were seldom investigated. Notably, the sway of diverse eccentric faults on UMP is pronouncedly disparate, and different UMP can transform dynamic performance of system under electromagnetic excitation, which have been shown in related researches [31–33]. Consequently, the vibration rule of shafting system under transient operating conditions can be clarified accurately and comprehensively, by virtue of incorporating static and dynamic

eccentricity (SDE) and associated UMP into the HMESS model, and carefully delineating the compositions of typical transient conditions, as well as carrying out qualitative and quantitative analyses, which is of great significance to bring a different perspective and expand current understanding, also provide reference for the dynamic analysis and fault diagnosis and identification of unit.

Motivated by these considerations, the novelty of present study can be summarized as: 1) Taking the start-up process as the research condition, and employing the UMP, which takes into account the influence of static and dynamic air gap eccentricity, as core electromagnetic excitation, and the connection among hydraulic, mechanical, electrical parameters and the vibration of unit through transient process of HMESSs is established. 2) On this basis, the dynamic properties of shafting system at different stages in start-up process are investigated. 3) The vibration response mechanisms of rotor and runner when system is in start-up scenario are clarified, by contrast with the vibration rule under steady-state operating condition, so as to provide salutary reference for the analysis of dynamic trait in coupled hydraulic-mechanical-electrical-structural system under unsteady-state operating conditions.

The rests of this paper are organized as follows: Section 2 presents the models of each subsystem from HGS and the mathematical modeling of HMESSs. Numerical simulation and dynamic behavior analyses of system parameters, the transient vibration peculiarity about rotor and runner during the start-up process, and the repercussion of electromagnetic excitation with static and dynamic eccentricity on rotor vibration response under the voltage building-up stage, are performed and revealed detailedly in Section 3. The discussion of the paper is emphasized in Section 4, including the limitations, the improvement suggestions and the future directions. Finally, in Section 5, the conclusions are summarized.

2. The transient model for HMESS

The HGS consists of upstream reservoir, penstock, volute, shafting system, plant, draft tube, downstream reservoir and power grid, as shown in Fig. 1, in which the red arrow indicates a schematic diagram of shafting system, including spindle, generator rotor, turbine runner, upper guide bearing, lower guide bearing, turbine guide bearing, flange and so forth.

The coupled hydraulic-mechanical-electrical-structural system of HGS, containing penstock subsystem, turbine subsystem, generator subsystem, governor subsystem and grid subsystem, is demonstrated in Fig. 2. In the operation of hydraulic generating set, various dynamic loads such as unbalanced magnetic pull, sealing force, oil film force and pulsating pressure are altered under the impact of transition process, affecting dynamic response of unit.

2.1. Penstock subsystem

In this paper, the one-dimensional (1D) penstock model with simple calculation and enough accuracy is selected to simulate the transient flow of penstock in hydropower system, and the method of finite difference and the method of characteristic (MOC) are employed for the solution [20,29].

Meshing and discretizing the momentum equation and continuum equation of 1D transition flow through the explicit difference format in finite difference method:

$$Q_i^{n+1} = \frac{1}{2} (Q_{i+1}^n + Q_{i-1}^n) - \frac{\Delta t Q_i^n}{2A\Delta x} (Q_{i+1}^n - Q_{i-1}^n) - \frac{\Delta t g}{2\Delta x} (H_{i+1}^n - H_{i-1}^n) - \frac{f}{8DA} (Q_{i+1}^n + Q_{i-1}^n) | (Q_{i+1}^n + Q_{i-1}^n) | \quad (1)$$

$$H_i^{n+1} = \frac{1}{2} (H_{i+1}^n + H_{i-1}^n) - \frac{\Delta t Q_i^n}{2A\Delta x} (H_{i+1}^n - H_{i-1}^n) - \frac{\Delta t}{2A\Delta x} \frac{a^2}{g} (Q_{i+1}^n - Q_{i-1}^n) - \frac{\Delta t}{A} Q_i^n \sin \alpha_1 \quad (2)$$

where Q and H are discharge and head of penstock, respectively; the subscripts i and n denote the position node i and time node n , severally; Δx is the space step; Δt is the time step; D means cross section diameter of penstock; A is the area of penstock; g is gravity acceleration; f is drag coefficient along the path; α is the angle between pressure pipe axis and horizontal plane; a_1 is water hammer wave velocity.

The upstream and downstream boundary conditions of penstock, as well as corresponding boundary equations are derived by MOC. The turbine represents the downstream boundary condition of penstock, whose positive characteristic equation at time step n is:

$$Q_{i+1}^{n+1} = A (C_p - C_a H_{i+1}^{n+1}) \quad (3)$$

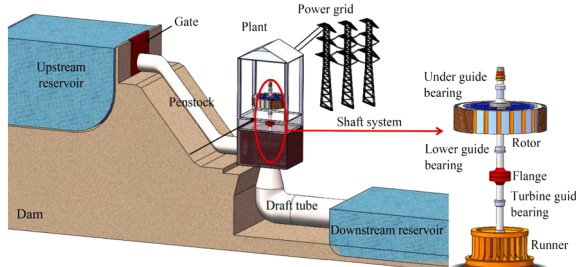


Fig. 1. Schematic diagram of hydroelectric generating system.

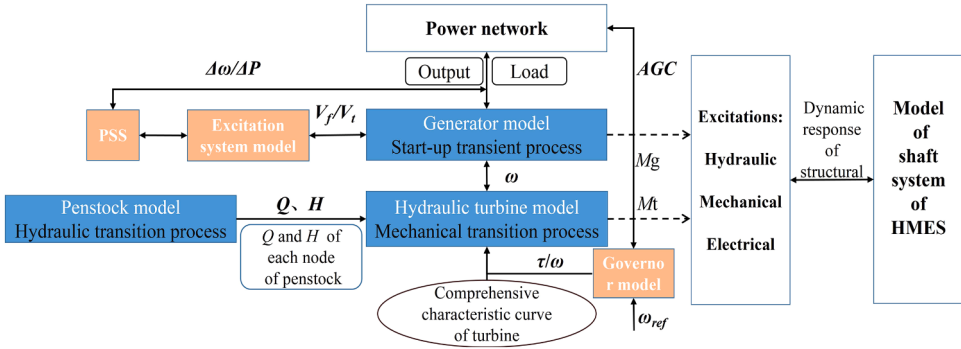


Fig. 2. The structure of coupled hydraulic-mechanical-electrical-structural system of HGS.

Besides, the reservoir is treated as the upstream boundary condition for penstock, and corresponding negative characteristic equation at time step n is given as:

$$Q_1^{n+1} = A(C_n + C_a H_1^{n+1}) \quad (4)$$

in which, C_a , C_p and C_n represent the coefficients associated with the Q , H and the geometry of penstock in previous time step [29], and the upstream head H_1 is given, the discharges and heads of all nodes in penstock system can be obtained by simultaneous solution of Eqs. (1) - (4).

2.2. Water turbine subsystem

The water turbine subsystem is connected to penstock subsystem and the turbine model is used to solve parameters in transient process, including operating head, discharge, etc. The operation status of water turbine is decided by rotational speed (ω), efficiency (η), discharge (Q) and opening (τ), while the hydraulic turbine performance curves (HTPC) just plays the role of representing the nonlinear relationship among the four variables mentioned above, as shown in Fig. 3, which is difficult to establish a mathematical expression providing with clear physical meaning, due to the highly nonlinear characteristic of the curves. Generally, the data required for the transient process calculation is usually obtained from HTPC utilizing the interpolation method. As the HTPC normally includes

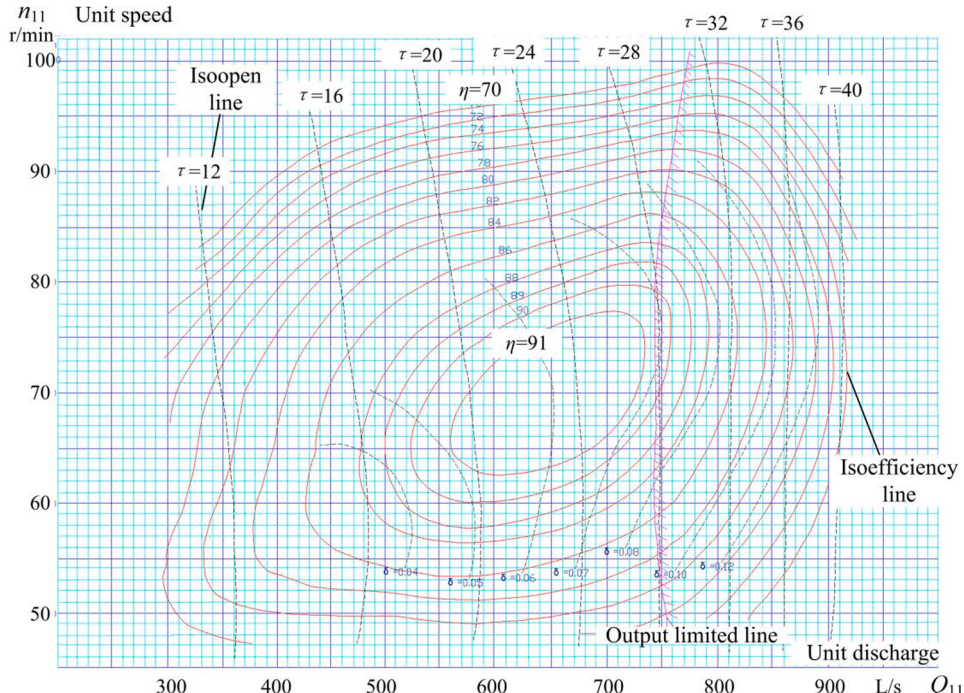


Fig. 3. Characteristic curves of hydraulic turbine model named as HL180-LJ-410.

data for high efficiency region based on model tests, so the basis and core segment of the simulation for water turbine transition process, becomes the acquisition of operating characteristic curves about turbine in small opening and low efficiency regions based on available data.

With sufficient number of learning sample points, the nonlinear mappings corresponding to these variables can be constructed and approximated infinitely with required accuracy, by the learning and reconstruction capability of neural network. The radial basis function (RBF) neural network method proposed in the Ref. [34], is adopted to fit and reconstruct the original HTPC in this paper. Firstly, the HTPC is expanded to large, small opening and high, low efficiency regions based on boundary conditions and engineering experience, for the obtainment of sufficient sample points for neural network learning. Subsequently, the RBF neural network for comprehensive characteristic curves of water turbine can be built by means of simulation function, namely Sim, in the neural network toolbox of MATLAB. Finally, the training network can be established via the neural network function, i.e. Newrb, the fitted discharge and efficiency comprehensive characteristic curves of turbine obtained are shown in Fig. 4 (in which “ \circ ” indicates the original known regions in HTPC).

The fitting results show that the maximum error in discharge is $0.367 \times 10^{-3} \text{ m}^3/\text{s}$ and the minimum is only $0.001 \times 10^{-3} \text{ m}^3/\text{s}$, which conform the accuracy requirements of engineering simulation calculations. The fitted turbine comprehensive characteristic curves data is digitally stored and can be queried according to calculation needs, so that the unit discharge, speed, opening and efficiency under diverse working conditions can be obtained quickly and accurately.

The rotating equation of turbine can be written as:

$$J \frac{d\omega_m}{dt} = J \frac{d^2\theta_m}{dt^2} = M_t - M_e \quad (5)$$

where J is the moment inertia of hydroelectric generating set; ω_m is mechanical angular velocity; θ_m is mechanical rotation angle; M_t and M_e mean the instantaneous rotational torque of turbine and generator, respectively.

Once the discharge, speed and guide vane opening are known for the previous time step, the net turbine head (H_{np}) and M_t can be solved by the iterative method. The relationship of the parameters, when the turbine is treated as a boundary condition, is demonstrated in Fig. 5, where H_{t1} is the difference in height from draft tube to base line, then, the turbine inlet head H_p can be expressed as:

$$H_p = H_{np} + H_{t1} - \frac{Q_p^2}{2gA^2} \quad (6)$$

The turbine inlet head (H_p) and inlet discharge (Q_p) are attained combining with the positive characteristic equation, and the τ for this time step is solved from governor model, while the obtainment of speed at this step needs assisted by acquiring the electromagnetic power in synchronous motor model.

2.3. Generator and grid subsystems

A third-order model of synchronous machine is adopted to simulate the generator subsystem, aiming to solve parameters of generator power (P_e), generator current (I) and voltage (U_G) in transition process. Considering the impression of power grid, the constant impedance model is hired to represent the load which fluctuates with voltage variation. According to the time-space vector diagram of steady-state motor, the time-space vector relationship for current and voltage of generator in the course of transient process

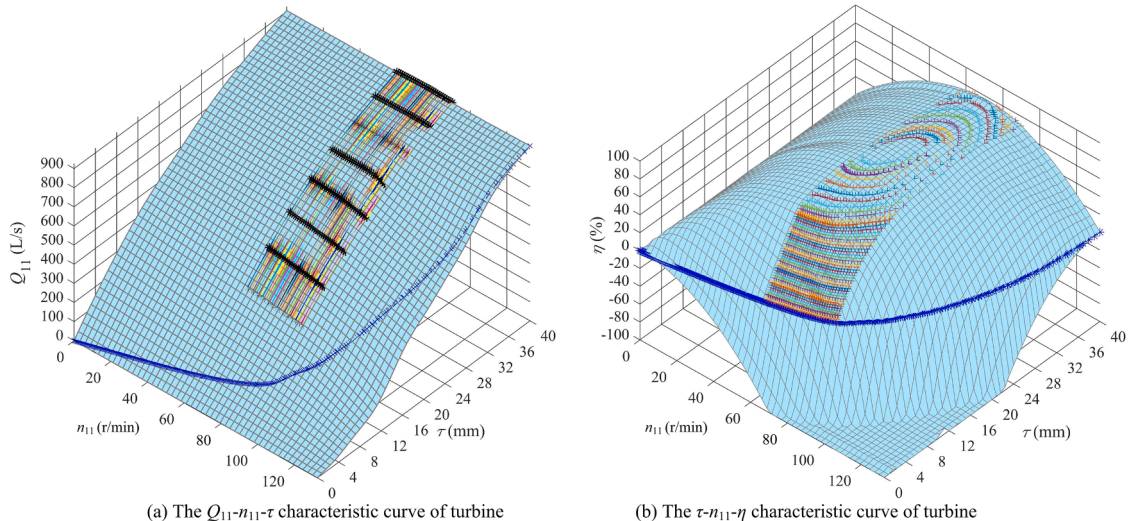


Fig. 4. Recomposed surface of $Q_{11}-n_{11}-\tau$ and $\tau-n_{11}-\eta$.

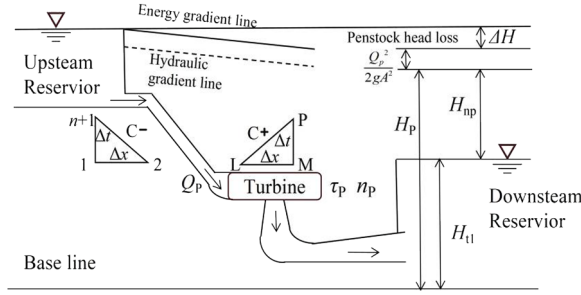


Fig. 5. Boundary conditions of Francis turbine.

is able to be obtained, as illustrated in Fig. 6, ultimately, the mathematical model of synchronous generator is derived combining with the motion equation of rotor, the current-voltage equation, the electromagnetic transient equation of excitation winding and power equation:

$$\left\{ \begin{array}{l} J \frac{\omega_{ms}^2}{\omega_{es}} \frac{d\omega_e}{dt} = (P_t - P_e - P_0 D_0 x) \frac{\omega_e}{\omega_{es}} \\ \frac{d\delta}{dt} = \omega_{es} \left(\frac{\omega_e}{\omega_{es}} - 1 \right) \\ T'_{do} \frac{dE'_q}{dt} = E_{fd} - E'_q - I_d (X_d - X'_d) \\ U_{Gq} = E'_q - I_d X'_d \\ U_{Gd} = I_q X_q \\ U_G^2 = U_{Gq}^2 + U_{Gd}^2 \\ P_e = U_{Gq} I_q + U_{Gd} I_d \end{array} \right. \quad (7)$$

where ω_e is the electrical angular velocity of generator rotor; ω_{es} is synchronous electrical speed; P_0 , P_t and P_e denote the rated power, mechanical power and electromagnetic power of generator, respectively; δ means power angle; X_d and X_q are the synchronous reactance of d - and q - component, respectively; X'_d is the transient reactance of d -component; I , I_d and I_q refer to the generator current and corresponding d - and q - components, respectively; E'_q is the transient electromotive force (EMF) of q -axis; $T'_{do} = (X_f/R_f)/\omega$ is the open-circuit transient time constant of d -axis; U_G , U_{Gd} and U_{Gq} are the stator terminal voltage and corresponding d - and q - components, severally; E_{fd} is the imaginary open-circuit EMF generated by field voltage; D_0 is damping factor.

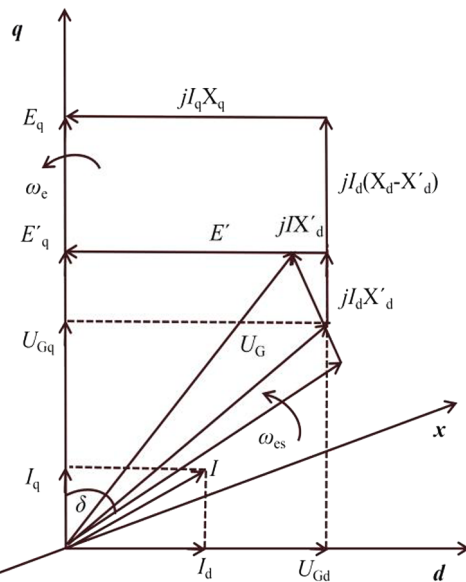


Fig. 6. Phasor diagram of the salient synchronous generator.

2.4. Governor subsystem

The PID governor model is applied to simulate the turbine speed varying with power load. The transfer function of frequency regulation mode is shown in Fig. 7, where C_f is given as frequency command, x is the input (deviation ratio of rotating speed) variable and y is the output (servomotor stroke) variable, and then, the transfer function from input to output can be expressed as:

$$G(s) = \frac{Y(s)}{X(s)} = \frac{K_D S^2 + K_p S + K_I}{b_p K_D S^2 + (b_p K_p + 1)S + b_p K_I T_y S^2 + T_y S + 1} \quad (8)$$

in which, K_p , K_I and K_D are the proportional, integral and differential gains of governor, respectively; b_p is permanent droop; T_y is servomotor response time constant; T_{yB} is reaction time constant of auxiliary servomotor; K is integrated amplification factor.

Through the inverse Laplace transformation, a third-order differential equation for the parallel PID type governor in frequency regulation mode is obtained:

$$b_p K_D T_y \ddot{y} + (b_p K_p T_y + T_y + b_p K_D) \dot{y} + (b_p K_I T_y + b_p K_p + 1) y + b_p K_I y = K_D \ddot{x} + K_p \dot{x} + K_I x \quad (9)$$

The third-order differential equation of the governor can be transformed into a differential equations of first order, with the help of modern control theory, and the fourth-order Runge-Kutta method is applied to solve the servomotor stroke and further obtain τ .

2.5. The shafting system model

The schematic diagram of shafting system for hydraulic generating set is depicted in Fig. 8, where B_1 , O , O_2 , B_2 , B_3 , O_3 indicate the centroid of upper guide bearing, generator stator, rotor, lower guide bearing, water guide bearing and turbine runner, respectively. For the purpose of facilitating analysis, it is assumed that $B_1 O = O B_2 = B_3 O_3 = B_2 B_3 / 2$ [35,36].

The air gap with compounded eccentricity between rotor and stator of generator, and coordinate partial magnification diagram are demonstrated in Fig. 9. O is the inner circle center of stator, S is the initial center of journal, the decentration of O and S is universal when system is stationary due to processing, assembly, etc., O_1 is the center of journal after deformation, G is the mass center of rotor, (X_1, Y_1) , (X_2, Y_2) are the centroid coordinates of rotor and journal, respectively. O_2 is the geometric center of rotor, $e_1 = GO_2$ is the mass eccentricity of rotor, $O_1 S$ is the eccentricity due to rotor vibration, OS is the static eccentricity, $O_1 O_2$ is the eccentricity owing to the decentration of rotor center and journal center, i.e. the dynamic eccentricity. α is the included angle between air gap position and x -axis, γ is the rotation angle of rotor center, φ is the rotating angle of mass center surrounding the geometric center, ω is the rotational angular speed, $\delta(\alpha, t)$ is the air gap length of rotor at arbitrary time.

To simplify calculations and facilitate comparisons, the UMP can be derived by the air gap permeability method, and the effect of distribution of magnetic pole on air gap permeability can be neglected. Taking the minimum air gap of stator and rotor as the origin of coordinates, the air gap length can be expressed approximately as [31]:

$$\delta(a, t) = \delta_o [1 - \delta_s \cos \alpha - \delta_d \cos(\alpha + \omega t)] \quad (10)$$

where δ_0 is average air gap length; δ_s and δ_d are static eccentricity and dynamic eccentricity of air gap, correspondingly.

Neglecting the higher order components of Eq. (10) and expanding the air gap permeance into Fourier series:

$$\Lambda(a, t) = \frac{\mu_0}{\delta(a, t)} = \Lambda_0 - \Lambda_s \cos \alpha - \Lambda_d \cos(\alpha + \omega t) \quad (11)$$

where μ_0 is air permeance; $\Lambda_0 = \mu_0 / \delta_0$ is the constant component of air gap permeance; $\Lambda_s = \Lambda_0 \delta_s$ and $\Lambda_d = \Lambda_0 \delta_d$ are magnetic conductivity components attracted by static and dynamic eccentricity, respectively.

In line with the theory of electric machine and Maxwell stress integral, the UMP can be deduced:

$$\begin{cases} F_{x_ump} = LR \int_0^{2\pi} q(\alpha, t) \cos \alpha d\alpha = \frac{LR F_1^2 \pi}{4\mu_0} \{2\Lambda_0 \Lambda_s + 2\Lambda_0 \Lambda_d \cos \omega t + \Lambda_0 \Lambda_d + \Lambda_0 \Lambda_s \cos(2\omega t - 2\beta) \\ F_{y_ump} = LR \int_0^{2\pi} q(\alpha, t) \sin \alpha d\alpha = \frac{LR F_1^2 \pi}{4\mu_0} \{2\Lambda_0 \Lambda_d \sin \omega t + \Lambda_0 \Lambda_d \sin(\omega t - \beta) + \Lambda_0 \Lambda_s \sin(2\omega t - 2\beta)\} \end{cases} \quad (12)$$

where L and R are the length and radius of rotor, respectively; F_1 is synthetic magnetomotive force amplitude of air gap; β is the coefficient of angularity [36].

Considering the hydraulic, mechanical, electrical time-varying loads covering the UMP with static and dynamic eccentricity, rub-impact force, oil film force, sealing force and eccentric force, the Lagrange equation is used to derive differential equations of rotor-

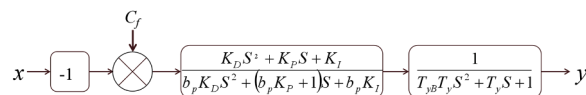


Fig. 7. Transfer function of frequency regulation mode.

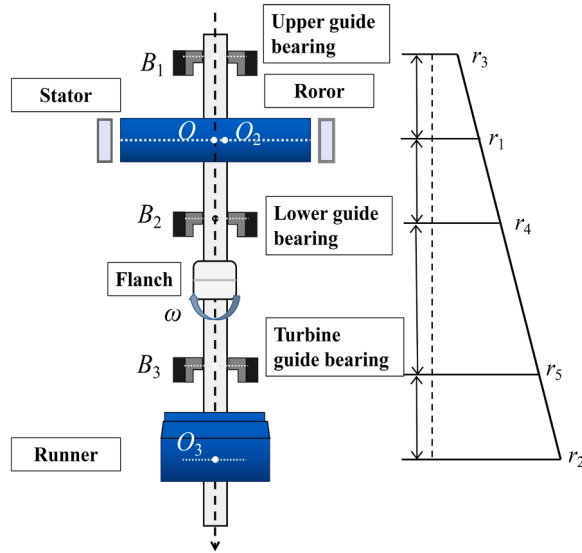
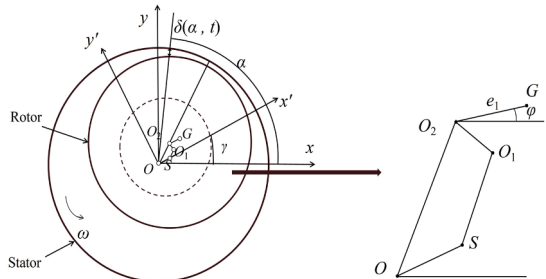


Fig. 8. Schematic diagram of shafting system of hydraulic generating set.



(a) Schematic diagram of air gap eccentricity (b) Coordinate partial magnification diagram

Fig. 9. Schematic diagram of air-gap with SDE rotor.

runner system for hydraulic generating set in this paper:

$$\left\{ \begin{array}{l} m_1 \ddot{X}_1 + c_1 \dot{X}_1 + K_1 (X_1 - X_2) = m_1 e_1 \left(\dot{\phi}_1^2 \cos \phi_1 + \ddot{\phi}_1 \sin \phi_1 \right) + F_{x-ump} + F_{x-rub} \\ m_1 \ddot{Y}_1 + c_1 \dot{Y}_1 + K_1 (Y_1 - Y_2) = m_1 e_1 \left(\dot{\phi}_1^2 \sin \phi_1 + \ddot{\phi}_1 \cos \phi_1 \right) + F_{y-ump} + F_{y-rub} \\ m_2 \ddot{X}_2 + c_2 \dot{X}_2 + \frac{1}{2} K_1 (X_2 - X_1) = f_x \\ m_2 \ddot{Y}_2 + c_2 \dot{Y}_2 + \frac{1}{2} K_1 (Y_2 - Y_1) = f_y \\ m_3 \ddot{X}_3 + c_4 \dot{X}_3 + K_2 X_3 = m_3 e_3 \left(\dot{\phi}_2^2 \cos \phi_2 + \ddot{\phi}_2 \sin \phi_2 \right) + F_x \\ m_3 \ddot{Y}_3 + c_4 \dot{Y}_3 + K_2 Y_3 = m_3 e_3 \left(\dot{\phi}_2^2 \sin \phi_2 + \ddot{\phi}_2 \cos \phi_2 \right) + F_y \\ (J_{p1} + m_1 e_1^2) \ddot{\phi}_1 + c_3 \dot{\phi}_1 + k_t \theta_1 = m_1 e_0 \left(\ddot{X}_1 \sin \phi_1 - \ddot{Y}_1 \cos \phi_1 \right) + M_{-ump} + M_{-rub} \\ (J_{p2} + m_3 e_3^2) \ddot{\phi}_2 + c_5 \dot{\phi}_2 + k_t \theta_2 = m_3 e_3 \left(\ddot{X}_3 \sin \phi_2 - \ddot{Y}_3 \cos \phi_2 \right) \end{array} \right. \quad (13)$$

in which,

Table 1

Data of system models.

Time constants of governor starting-up (s)											
T_m	T_w	T_d	T_n	b_p	b_t	T_{do}	T_e	T_y			
9	1.10	15	0.6	0.005	0.6	3	1	0.1			
Parameter value of rotor-bearing system (m)											
R_a	R_b	R_i	R_o	L_p	c_r	c_b	$c_1(\text{N.s/m})$	$c_2(\text{N.s/m})$	$J_{p1}(\text{kg.m}^2)$	$k_1/k_2/k_3(\text{N/m})$	
0.9	2.12	2.120	2.185	0.587	0.018	0.36e-3	4.3e5	3e5	2.592e4	8.5e7/6.5e7/3.5e7	
Nominal/no-load value of excitor and generator											
I_f (A)	I (KA)		U_G (KV)	$\cos\varphi$	U_L (KV)	$m_3(t)$	p	e_1 (mm)	R (m)	L (m)	
1300/850 [#]	4.32 [#] /0		13.8 [#]	0.885	12.21	144	12	0.7	5	2.5	
Nominal/no-load value of turbine											
H (m)	Q (m^3/s)		P_t (KVA)	ω (r/min)	$m_3(t)$	$J_{p2}(\text{kg.m}^2)$	e_3 (mm)	D_1 (m)	L/D (m)	$c_3(\text{N.s/m})$	
116.2/124.9 [#]	90.57/14.7		103.4 [#] /0	150 [#]	112	2.016e4	4.5	4.1	495/8.5	5e5	

$$K_1 = \frac{1}{16} \left[(25k_1 + 9k_2 + k_3) + (-5k_1 + 3k_2 + 3k_3) \frac{\sqrt{x_3^2 + y_3^2}}{\sqrt{x_1^2 + y_1^2}} \right]$$

$$K_2 = \frac{1}{16} \left[(k_1 + k_2 + 9k_3) + (-5k_1 + 3k_2 + 3k_3) \frac{\sqrt{x_1^2 + y_1^2}}{\sqrt{x_3^2 + y_3^2}} \right]$$

where m_1 , e_1 , φ_1 , J_{p1} , m_3 , e_3 , φ_2 and J_{p2} are the mass, mass eccentricity, rotation angle and rotational inertia of rotor and runner, respectively; k_1 , k_2 and k_3 mean the stiffness of upper, lower and water guide bearing, separately; $F_{x,rub}$, $F_{y,rub}$ and M_{rub} are the components of the rub-impact force in x , y direction and the frictional moment, respectively; f_x and f_y are the nonlinear oil film force components; F_x , F_y are the nonlinear sealing force components; M_{ump} is the electromagnetic torque [37].

3. Numerical analysis

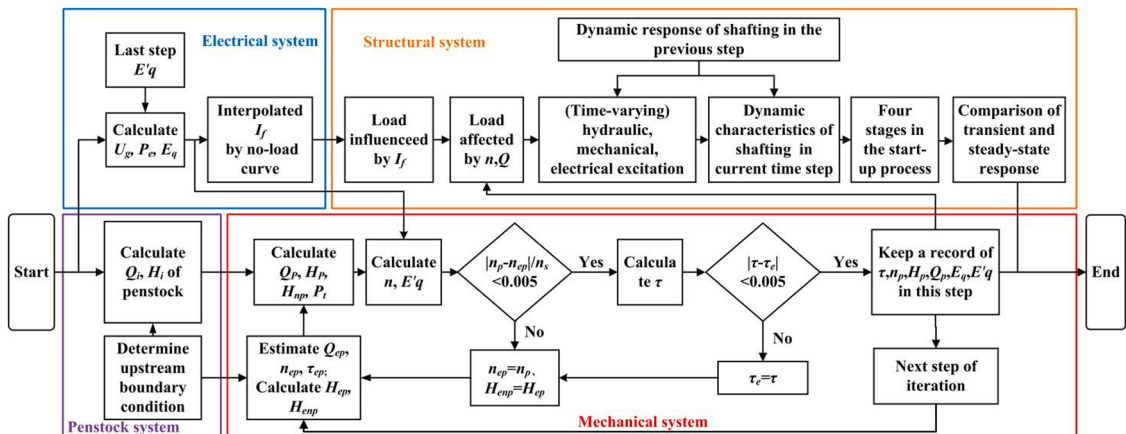
The hydraulic turbine model named as HL180-LJ-410 conforming to the Chinese design criteria, is selected as the object in this paper to simulate the start-up process of HGS, which means a Francis turbine whose specific speed is 180 m·KW, vertical arrangement, metallic volute, and the nominal diameter of runner is 410 cm. The duration of start-up process for numerical simulation is 43s, and the process of voltage building-up for generator begins at $t = 27$ s when rotating speed, output and discharge of water turbine have been stabilized. The essential parameters involved in the calculation including penstock, governor, generator and excitation systems, are listed in Table 1, where “#” indicates the basic value of per unit.

Based on the introduction of subsystem models, the solving process of dynamics model for HMESS can be expressed in Fig. 10, with the specific calculation process as follows:

- (1) Determine initial values of upstream boundary conditions H_1 , Q_1 .
- (2) Calculate H_i and Q_i of each point in penstock model, using the finite difference method and MOC in combination with step (1).
- (3) Determine the initial values n_{ep} , Q_{ep} , H_{ep} and τ_{ep} for the current iteration step, and calculate turbine power P_t with characteristic curves and similarity law of water turbine.
- (4) Solve P_e , E_q and U_G with third-order motor model, excitation equation, grid equation and previous time step $E'q$.
- (5) Resolve n_p from Eq. (7), and verdict whether the inequality $|n_p - n_{ep}|/n_s < 0.005$ is satisfied: a) Yes, continue the calculation; b) No, return to step (3) for calculation again with n_p , Q_p and H_{np} as iterative values.
- (6) Determine τ from Eq. (9) and estimate whether the inequality $|\tau - \tau_{ep}| < 0.005$ is satisfied: a) Yes, continue the calculation; b) No, return to step (3) for calculation again with τ and the result from step (5), as iteration values.
- (7) Calculate the loads generated by hydraulic, mechanical and electrical excitation sources, solve the dynamic characteristic of shafting system.
- (8) Record the results and go to step (1) for next time step until convergence.

3.1. The variation property of system parameters

The variation properties of ω , I_f , P_t , H and Q of unit over the start-up process are illustrated in Fig. 11. In order to clearly reflect and facilitate the dynamic characteristic analysis of unit, the start-up process is divided into four stages according to the variation law



Note: The subscript of ep represents the estimated value of the parameter; the subscript of p represents the calculation value in current time step.

Fig. 10. Computational process of the system.

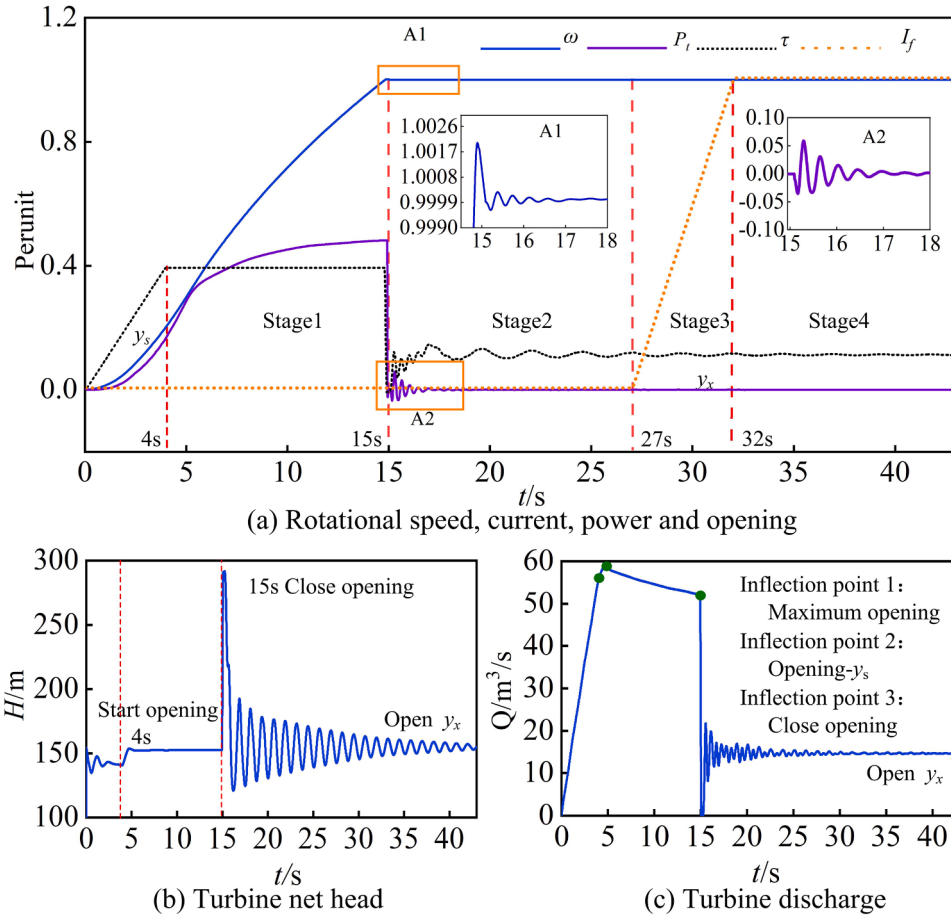


Fig. 11. Fluctuation curves of parameters over start-up process.

of ω and I_f (as depicted in Fig. 11 (a)): Stage 1 [0~15s]; Stage 2 [15s~27s]; Stage 3 [27s~32s]; Stage 4 [32s~43s]. It can be seen that in the period of start-up, system parameters have the following patterns in four stages:

- (1) After receiving the starting command, the governor adjusts τ from zero to starting value $y_s = 0.4$ within 4s, while the output power of turbine moderately elevates at the initial stage. Once turbine torque exceeds friction torque M_f , the turbine starts to rotate and M_t reaches the maximum value when $\tau = y_s$, and then M_t descends gradually with the continuous rise of ω . Subsequently, the τ stabilizes at rated value ($t = 4\text{--}15$ s), in which Q decreases, resulting in a slow growth of power. At this stage, ω rises smoothly with barely appearing overshoot phenomenon.
- (2) The system enters Stage 2 when ω reaches to nominal value of static characteristic for governor, the τ begins to attenuate and finally keeps stable with a constant no-load value ($y_x = 0.12$). Once ω stabilizes, i.e. $d\omega/dt = 0$, the P_t decreases to zero after

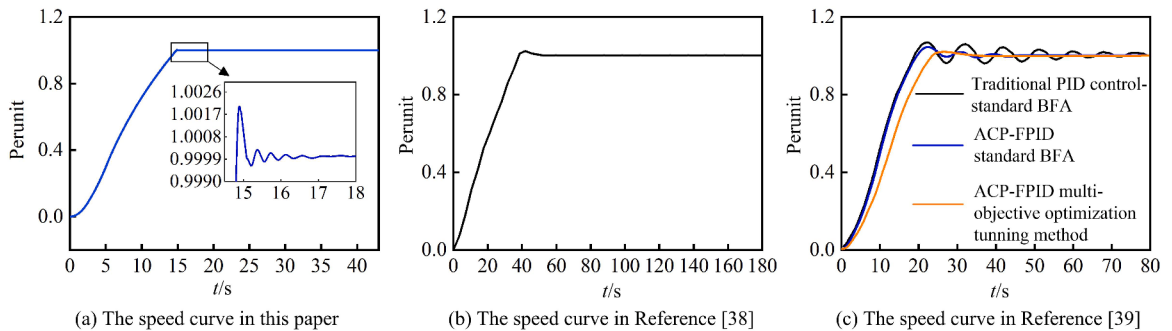


Fig. 12. Comparison of speed during start-up process.

experiencing a short variability process. The H is varying with the alteration of τ and Q , the turbine head decreases as a suddenly upsurge of τ , and the H rises instantly with rapid closure of τ . Since the unit is in no-load condition, the actual head will be smaller than static head before unit is started, while the difference is hydraulic loss, at this time, $\Delta H < 0$.

- (3) The voltage building-up stage of generator initiates at $t = 27$ s among the start-up process. The excitation current ascends drastically, the ω and P_t remain steady, while τ , H and Q fluctuate within a narrow range.
- (4) The excitation current rises to rating value of 850.9 A at $t = 32$ s, thereafter, as time increases the I_f no longer varies and other system parameters remain stable, the system enters a temporary steady-state stage until the end of start-up process. As the hydraulic generator set is not connected to the grid in the course of start-up process, the braking torque equals zero, i.e. $M_g = 0$.

The overall variation property of parameters such as ω , τ , P_b , H and Q over start-up process is consistent with that in References [38–40], as depicted in Fig. 12. In consequence, the model established in this paper can reflect the dynamic characteristic of transient process for hydraulic generating set.

3.2. The transient vibration analysis

The time history curves of rotor and runner displacement in the course of start-up process are presented in Fig. 13, obviously, there exists dissimilarity of the amplitude on two structures in four stages, due to different external excitation. Once system receives starting command, the instantaneous acceleration of ω under the control of PID governor adjusts with small increments, and the axis trajectory of rotor and runner hovers near the origin (as demonstrated in Fig. 14 (a)). The system is mainly subjected to mechanical eccentric force at the moment, and corresponding eccentric load is limited under low speed condition, hence, the system exhibits stable running trajectory within $t = 0\text{--}3$ s. When $t > 3$ s, the displacements of rotor and runner augment continuously with the rapid growth of ω , the

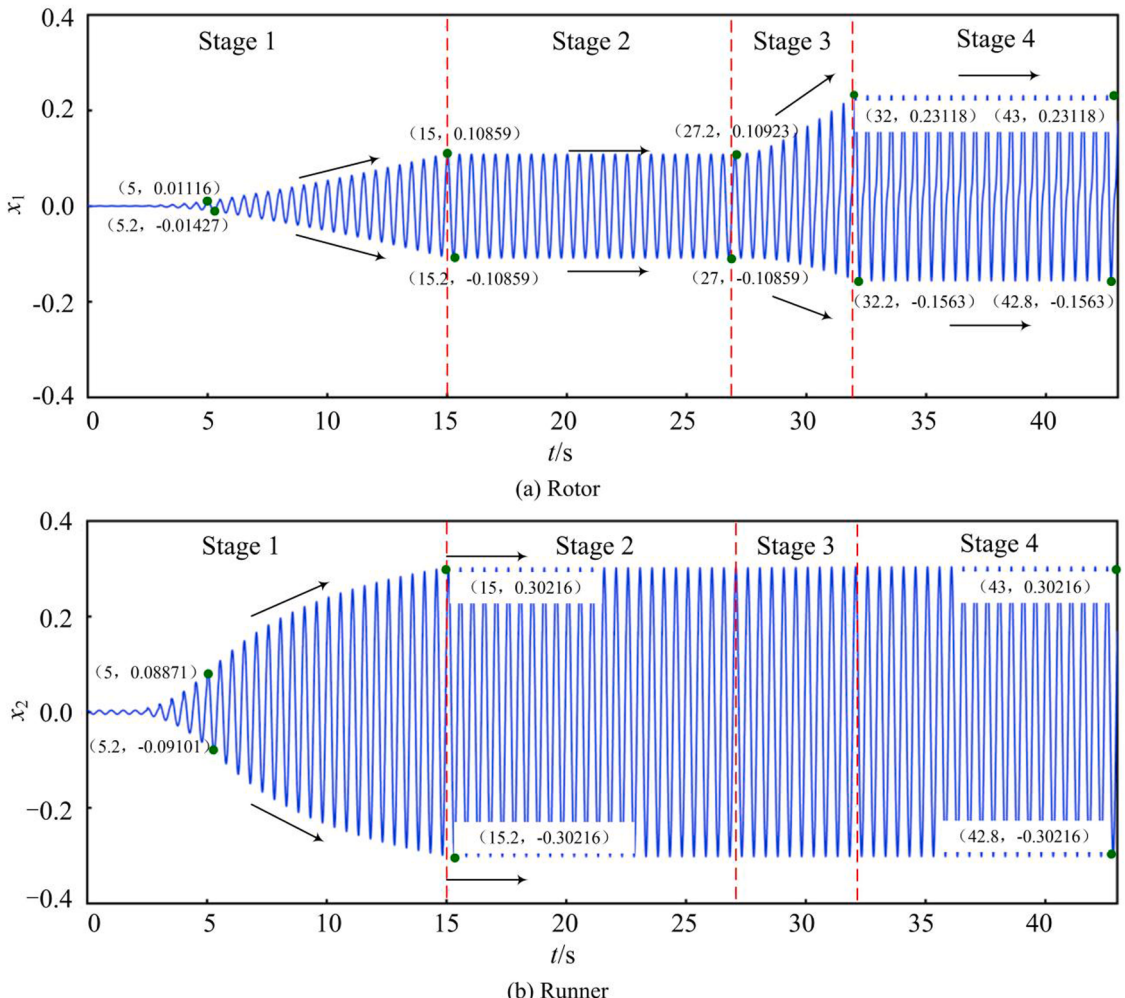


Fig. 13. The time history curves of rotor and runner displacement over start-up process.

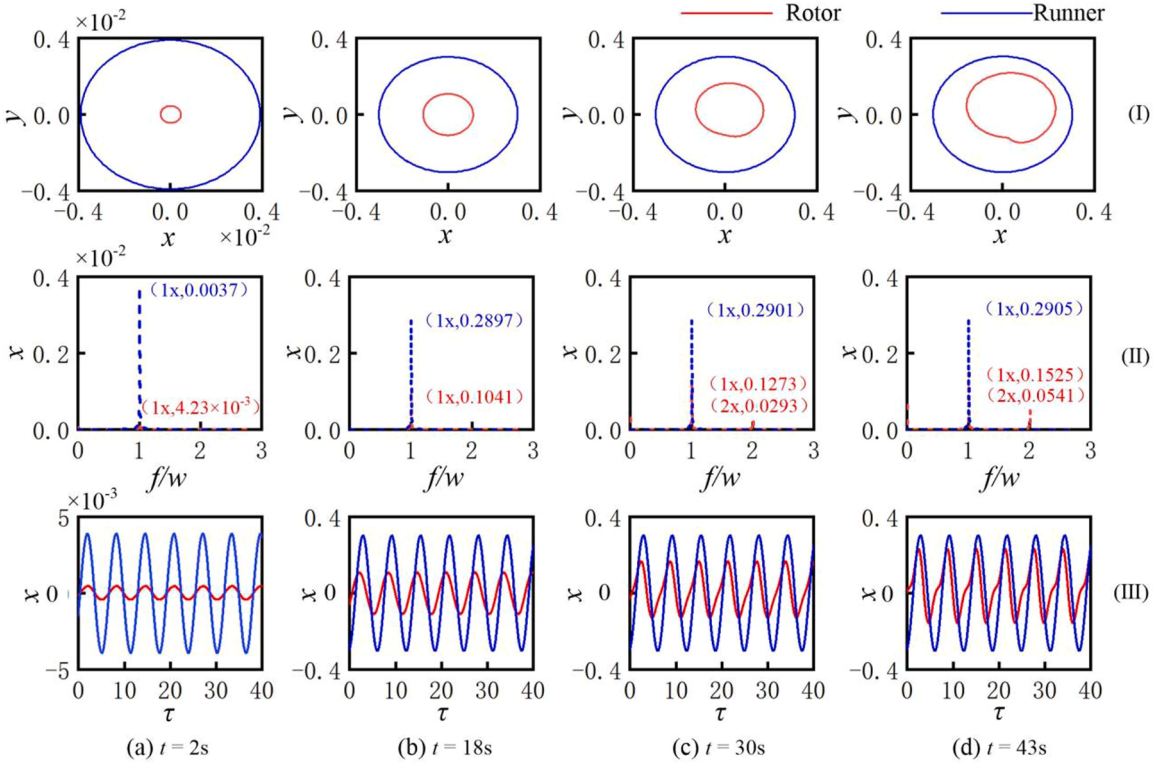


Fig. 14. The axis trajectory, spectrum and time domain diagrams of rotor and runner during start-up process.

displacements reach extreme value of 0.10859 and 0.30126, respectively, when ω equals rated point ($t = 15$ s), at which the displacement of runner is triple as high as that for rotor, as shown in Fig. 14 (b). On the one hand, the mechanical external excitation acting on runner is greater than that of rotor, due to the disparate initial eccentricities. On the other hand, at this stage, the rotor is only affected by unbalanced force without excitation current, while the runner is influenced with eccentric force and the dominant nonlinear sealing force ($t = 15$ s: $F_{eccentric} = 15.80 \times 10^4$ N, $F_{seal} = 33.39 \times 10^4$ N), resulting in more significant vibration of runner.

In Stage 2, the unit keeps running at rated speed, Q , P_t and τ are stable at rated values. The excitation exerting on rotor and runner is relatively invariable and the unit runs smoothly. The trajectory of rotor and runner maintains regular circular shape, and corresponding time domain diagrams are all in simple harmonic form (Fig. 14 (b)).

The voltage building-up process begins at $t = 27$ s, the excitation current grows rapidly and reaches nominal value within 5s, meanwhile, the rotor displacement is soaring and the matching trajectory is no longer regular circle. In addition to 1x frequency component, 2x frequency element is presented in the spectrum diagram of rotor, and related peak is about 1/4 of 1x frequency, as shown in Fig. 14 (c), while relevant time domain curve converts from a smooth simple harmonic curve in Stage 2 to two slopes of

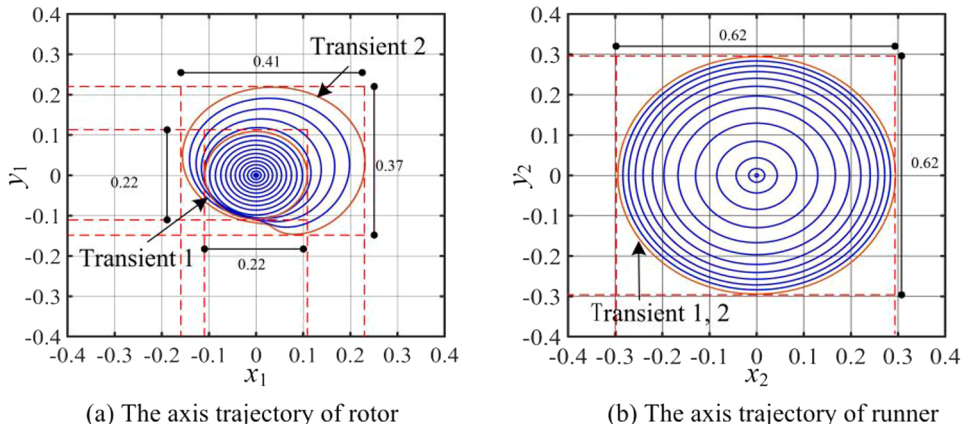


Fig. 15. The axis trajectory of rotor and runner during start-up process.

different curvature, and the harmonic period remains unchanged but the amplitude elevates, as depicted in Fig. 14 (III). The root cause is the different UMP amplitudes of rotor in x and y directions ($t = 30$ s: $F_x = 0.87 \times 10^4$ N and $F_y = 2.53 \times 10^4$ N), which leads to the destruction of the regularity on rotor trajectory. For the runner, the external excitation is relatively stabilized, although the rotor vibration is intensified by the time-varying UMP through voltage building-up process, the trajectory of runner remains stable due to the long distance between rotor and runner, as well as the protective effect of turbine guide bearing.

The voltage building-up process is ended at $t = 32$ s and the excitation current reaches nominal value. The constant excitation current, discharge and speed ensure a stable amplitude of UMP and a dynamic equilibrium relationship among UMP and rotor displacement, sealing force and runner displacement, furthermore, the rotor and runner enter a temporary stable operation again. The transient trajectory of rotor and runner during the start-up process is shown in Fig. 15, in which Transient 1 refers to the state before unit enters voltage building-up stage after reaching rated speed (Stage 2), and Transient 2 means the state that voltage building-up stage is completed and the unit is in no-load operation (Stage 4). The dynamic characteristic of rotor and runner is closely related to the damping and stiffness coefficients, and corresponding trajectory maintains fixed running track (Transient 2), when the system parameters and additional forces of shafting system barely fluctuate, i.e. the voltage building-up process is over until the load increase process appears, as displayed in Fig. 15. Apparently, the voltage building-up process throws a greater impact on rotor, which mainly falls into following aspects: the axis trajectory and vibration amplitude of rotor are significantly revised, the regularity of track is disrupted accompanied by approximately double amplitude, on the contrary, the influence on runner is negligible.

3.3. The effect of electromagnetic excitation with static and dynamic eccentricity

From the above analysis, it can be seen that the electromagnetic excitation imposes a significant influence on the vibration characteristic of rotor in voltage building-up process, while UMP is the nonlinear function about static and dynamic air gap eccentricity, moreover the fluctuation of both eccentricities will mutate the air gap permeability between stator and rotor, and further alter the amplitude of electromagnetic excitation. Since electromagnetic excitation exists after the voltage building-up process, the interval of $t = 27\text{--}43$ s among the start-up process is chosen for analysis. In addition, the operating state of runner after Stage 3 remains a steady state, thus, only the oscillation property of rotor is analyzed in this section.

The transient trajectory of rotor under the influence of generalized eccentricity (GE) [34], SDE, as well as the matching UMP amplitude curves, after the unit enters voltage building-up stage, are illustrated in Fig. 16. The excitation current and associated electromagnetic force are developing with the evolution of time, while the unit gets access to Stage 3, meanwhile, the displacement amplitude of rotor, under the actions of UMP with generalized eccentricity (GE-UMP) and UMP subjected to static and dynamic eccentricity (SDE-UMP), are rising continuously, as represented in Fig. 16 (a) and (b), nevertheless, the impact of two UMPs on system is significantly distinguishing. Firstly, the rotor amplitude suffered from the impact of SDE expands quicker than the former, accordingly, the maximum displacement is 0.2027, while the identical index of rotor with GE-UMP is 0.1283, as depicted in Fig. 16 (a) and (b), which clearly indicates that the effect of SDE-UMP is more prominent. What's more, the rotor trajectory gradually deviates from central position and distorts into an irregular closed ring, accompanied by a difference of amplitude in x and y direction, due to the addition of SDE, while the trajectory of rotor when GE-UMP is contained, is in a regular circular shape invariably. Combined with Fig. 17, it can be observed that there exists significant dissimilarity in the spectrum diagram of rotor, whether SDE are considered or not. For generalized eccentricity, only 1x frequency component is presented in the course of voltage building-up, and related amplitude is magnified with the intensification of electromagnetic excitation. Due to the existence of SDE, the 1x and 2x frequency components are displayed in spectrum diagram, and the proportion of 2x frequency is gradually enlarged, which leads to the alternation in rotor trajectory.

Obviously, the original vibration characteristic of system is altered as the addition of compound eccentricity. The static and dynamic eccentricity between rotor and stator is an inevitable failure in engineering practice, furthermore, the influence of induced electromagnetic excitation cannot be ignored, consequently, the impact of static and dynamic eccentricity on the vibration quality of rotor will be investigated separately in the subsequent part. The transient trajectories of rotor with different static and dynamic eccentricities, when the system undergoes voltage building-up process, are depicted in Fig. 18, as the depiction indicates, the vibration

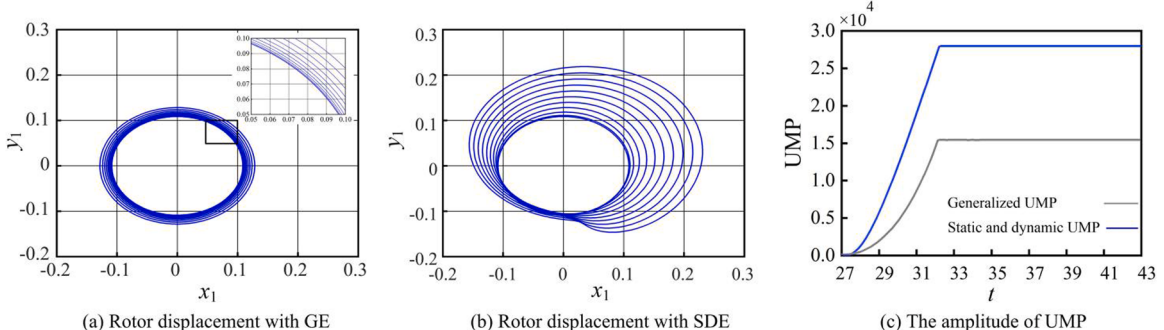


Fig. 16. The axis trajectory and matching UMP of rotor during voltage buildup process.

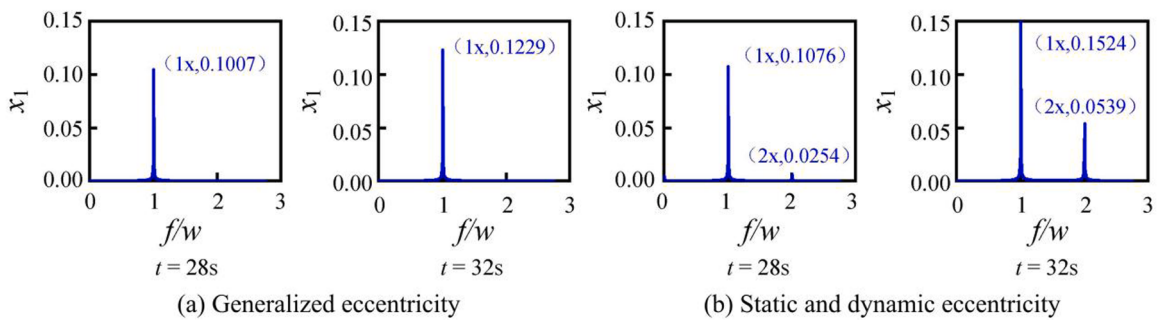


Fig. 17. Spectrum diagram of rotor at different time during voltage buildup process.

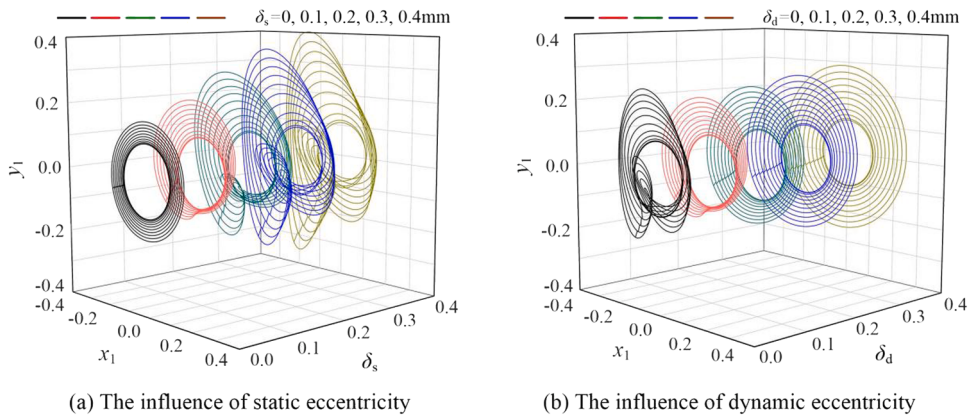


Fig. 18. Trajectory diagram of rotor under different static and dynamic eccentricities.

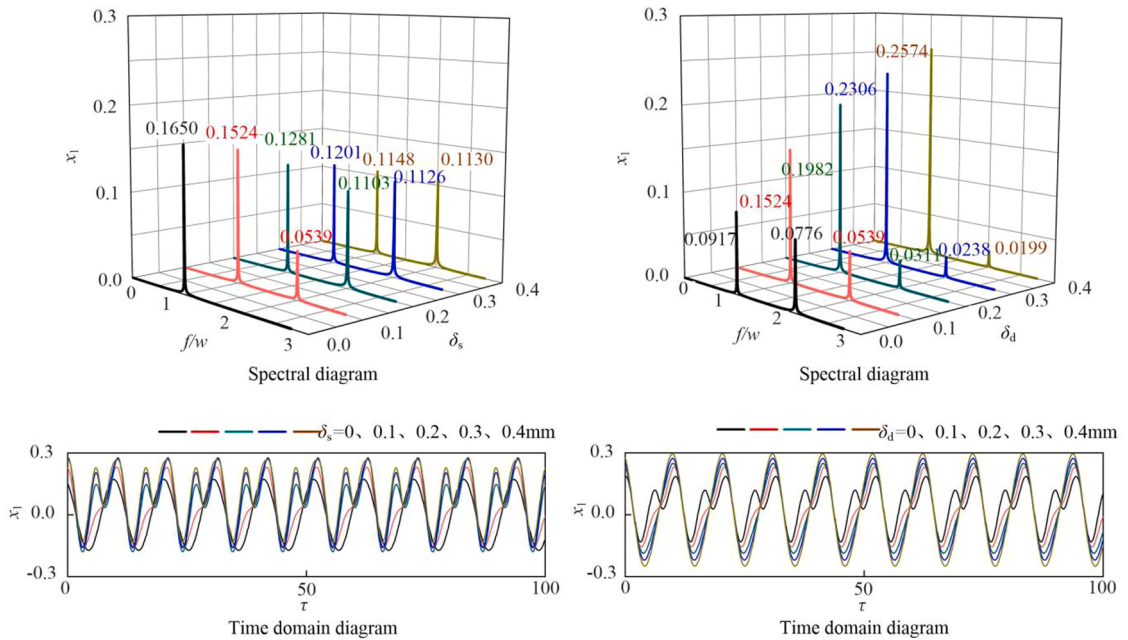


Fig. 19. Time domain and spectral diagrams of rotor with different eccentricities under no-load operation state.

amplitude of rotor shows a rising trend with the aggrandizement of two eccentricities, and the trajectories tend to be stabilized when excitation current reaches value of rating. It should be noted that, the influence patterns on rotor motion of static and dynamic eccentricity are discrepant, as evidenced by the following:

- (1) Firstly, the amplitude and trajectory of rotor are remodeled with the deterioration of static eccentricity. As illustrated in Fig. 18 (a), a significant increment in maximum transient displacement of rotor can be seen, from 0.1722 to 0.3960. Besides, the track of rotor evolves from a closed circle to an interwoven butterfly curve, meanwhile the motion center gradually deviates from original position, indicating that the regularity of trajectory is destroyed. Regarding the dynamic eccentricity, the amplitude of rotor expands with the evolution of δ_d , and the maximum transient displacement of rotor aggrandizes about 33% (from 0.2164 to 0.2893), as shown in Fig. 18 (b). In addition, the trajectory of rotor is increasingly regularized from an asymmetric annular curve to a regular circle, and the motion center is converged to the origin.
- (2) The time domain and spectral diagrams of rotor with different eccentricities are delineated in Fig. 19. As can be seen from the picture, the addition of static eccentricity prompts the appearance of 2x frequency component in spectrum diagram of rotor, the amplitude of 1x frequency reduces gradually with the deterioration of δ_s , while the proportion of 2x component progressively ascends and the matching dominant role becomes increasingly significant. And the corresponding time domain diagram is composed of two frequency components, which carries increasing trend in the amplitude of both dominate wave as well as harmonic wave, as drawn in Fig. 19 (a). In contrast to static eccentricity, the amplitudes and proportions of 1x and 2x frequency components in spectrum diagram, show opposite trends as δ_d burgeons. The period of vibration signal in time domain diagram of rotor remains fixed, and the harmonic component reduces gradually while the amplitude of dominate wave develops continuously, as presented in Fig. 19 (b). As discussed above, the static eccentricity will enhance the dominant role of 2x frequency and weaken the influence of 1x frequency, while the dynamic eccentricity will make the dominant role of 1x frequency more obvious, and moderate the role of 2x frequency, which is responsible for the progressive irregularity or regularity of rotor trajectory.

In summary, the amplification in either static or dynamic eccentricity of generator rotor among the transient process of HGS, will continuously strengthen the UMP, which intensifies the transient displacement of structure. The existence of UMP is equivalent to adding a negative stiffness to each guide bearing, reducing the inherent frequency of radial vibration of unit, and magnifying the multiplicative resonance amplitude of system as the eccentricity augments, as well as altering the nonlinear dynamic behavior from unit. However, the two eccentricities present different types from influencing on system when the system is in voltage building-up stage, the static eccentricity will trigger the 2x frequency electromagnetic excitation component, prompting the alteration of dynamic trajectory and the significant escalation in amplitude of rotor, while the dynamic eccentricity will aggravate the dominant role of 1x frequency electromagnetic excitation, impinging upon the vibration amplitude at multiplicative resonance of system, yet the dynamic trajectory of rotor will tend to be regular.

4. Discussion

Hydropower is applied to regulate the dynamic balance of grid capacity and frequency, due to the fast and efficient start-stop response. With the increasing proportion of clean energy in power grid, as well as the irregular grid-connections of renewable energy, represented by wind and photovoltaic power leading to the instability of grid, the operation conditions of hydroelectric generating system are bound to shift rapidly and frequently. The transformation of unit operation modes are usually accompanied by the fluctuation of hydraulic, mechanical, electrical parameters, which aggravates the uncertainty of hydraulic generating set. The excitation loads acting on unit are invariably in a state of transmutation over the transient process, especially the electromagnetic excitation, UMP, which is a nonlinear function related to excitation current and air gap eccentricity. The effect of electromagnetic excitation, attributed to both static and dynamic eccentricity, on the research of transition process for hydroelectric generating system was scarcely discussed in previous studies. The relevant researches show that, the addition of compound eccentricity results in certain influence to the vibration characteristic of system. In engineering practice, the SDE between rotor and stator is unpreventable, and the variation from excitation current, air gap eccentricity and other parameters will last, while the unit undergoes transient conditions such as start-up, load increase or decrease, shut-down and load rejection, the resulting electromagnetic excitation will have unexpected effect on the dynamic response of unit at different stages. Therefore, subdividing the transition process like start-up period into sub-intervals according to the development direction, meanwhile, fully taking the influence of potentially critical factors on the premier excitation sources into account, the dynamic feature of shafting system from overall and local transient operation is more likely to be precisely reflected, so as to provide reliable references with the accurate identification of vibration performance and fault types for unit.

It should be noted that, owing to the broad knowledge structure involved in the research of transient process for HGS, there still remains some limitations in this work, and the following aspects need to be further investigated and expanded in depth:

- (1) From the perspective of theoretical modeling and numerical simulation, the nonlinear dynamic characteristics of HGS is investigated in this paper, nevertheless, due to the limitations of time, personnel, site as well as funds, the authors are not able to carry out relevant experimental research. Once the time is ripe, we will expand the research based on this paper from the experimental verification level to form a comparison between numerical simulation and experimental analysis.

- (2) In this paper, the lumped parameter method is employed to establish the model of shafting system, and the model is simplified to a certain extent. Based on the finite element method to launch the dynamic response investigation of the shafting system under transient process, the corresponding vibration law of the system can be unearthed meticulously. Furthermore, with regard to the turbine runner, only the nonlinear sealing force is considered in this paper, and the introduction of the core hydraulic vibration source caused by the low-frequency vortex zone of draft tube and the Carmen vortex train, as well as the reasonable impose mode of the related hydraulic excitation on the runner structure, are valuable initiatives to further improve the system model constructed in this paper.
- (3) The dynamic properties of the hydropower plant structure under the start-up condition are not analyzed due to the space limitation. As an essential part of hydropower station, the vibration characteristics of typical structures such as generator floor, electrical floor, turbine floor, roof frame, stator foundation, wind shield and pier, are crucial for the safe and stable operation of the hydropower station, as well as the personal safety for the power station staff. Consequently, it is imperative to consider the unit and the plant structure as an integral system and incorporate the transient process into the research framework, so as to gain a profound understanding on the vibration pattern of the coupled unit-plant structure system under transient operating conditions.

5. Conclusions

Based on the construction of coupled hydraulic-mechanical-electrical-structural dynamic model for HGS, considering the influence of electromagnetic excitation under the action of static and dynamic air gap eccentricity, the dynamic response property of shafting system at different stages from the start-up process is analyzed in this paper. The results show that:

- (1) the dynamic operating laws of rotor and runner are significantly distinguishing in each period of start-up stage, due to the discrepancies in external excitation and position, the vibration amplitude of rotor tends to be escalated as the start-up process advances, the amplitude maintains stable after the speed stabilized until the voltage building-up stage ($t = 15\text{--}27\text{ s}$), and then ascends with the increase of excitation current in voltage building-up process, the vibration re-enters a stationary state after $t = 32\text{ s}$ (with a maximum amplitude of 0.2312); while the vibration amplitude of runner continues to escalate in the ramp-up stage, and the maximum amplitude halts at 0.3021 after the speed is stabilized.
- (2) Meantime, different dynamic phenomena of rotor structure from the system without compound eccentricity are revealed, due to the variation of UMP (the amplitude enlarged continuously, with the maximum addition of 81.74%), induced by static and dynamic air gap eccentricity in voltage building-up stage, including the disturbance of trajectory, the upsurge of vibration amplitude as well as the addition of spectral components.
- (3) In contrast to dynamic eccentricity, the alteration in dynamic response characteristic of system caused by static eccentricity in the voltage building-up process, is more outstanding, and the maximum transient displacement increases by nearly 130% (the corresponding index is 33% under the effect of dynamic eccentricity).

In practice, sufficient attentions should be paid to the influence of electromagnetic excitation affected by static and dynamic eccentricity in the start-up process, especially the voltage building-up stage, so as to ensure the safety and stability of hydraulic generating set under unsteady operating conditions.

CRediT authorship contribution statement

Jinjian Zhang: Conceptualization, Methodology, Software, Writing – original draft. **Zhenyue Ma:** Writing – review & editing, Data curation. **Xueni Wang:** Visualization, Formal analysis. **Qianqian Wu:** Supervision, Writing – review & editing. **Leike Zhang:** Supervision, Software, Funding acquisition.

Declaration of Competing Interest

The authors declare that they have no known competing financial interests or personal relationships that could have appeared to influence the work reported in this paper.

Data availability

Data will be made available on request.

Acknowledgments

This research paper is supported by the National Natural Science Foundation of China [grant number 51709196, 52379091]; the Basic Research Programs of Shanxi Province [grant number 202103021224086, 202203021222112].

References

- [1] X. Huang, W. Chen, Y. Wang, W. Wang, *World Energy Blueprint: World Energy Development Report*, Social Sciences Academic Press, Beijing, 2022, p. 2022.
- [2] Z. Zhao, X. Ding, P. Behrens, J. Li, M. He, Y. Gao, G. Liu, B. Xu, D. Chen, The importance of flexible hydropower in providing electricity stability during China's coal phase-out, *Appl. Energ.* 336 (2023), 120684, <https://doi.org/10.1016/j.apenergy.2023.120684>.
- [3] B. Xu, J. Zhang, M. Egusquiza, D. Chen, F. Li, P. Behrens, E. Egusquiza, A review of dynamic models and stability analysis for a hydro-turbine governing system, *Renew. Sust. Energ. Rev.* 144 (2021), 110880, <https://doi.org/10.1016/j.rser.2021.110880>.
- [4] Y. Sawle, S.C. Gupta, A.K. Bohre, Review of hybrid renewable energy systems with comparative analysis of off-grid hybrid system, *Renew. Sust. Energ. Rev.* 81 (2) (2017) 2217–2235, <https://doi.org/10.1016/j.rser.2017.06.033>.
- [5] H. Wei, A simulation model for evaluating Tianhuangping pumped storage hydro-plant, *Renew. Energy* 11 (2) (1997) 263–266, [https://doi.org/10.1016/S0960-1481\(96\)00046-8](https://doi.org/10.1016/S0960-1481(96)00046-8).
- [6] Q. Zhou, L. Xia, C. Zhang, Y. Yuan, Z. Zhu, Transient pressure fluctuations and runner loadings of a model pump-turbine during a load rejection process, *J. Hydraul. Eng.* 49 (11) (2018) 1429–1438, <https://doi.org/10.13243/j.cnki.slxb.20180706>.
- [7] R. Negru, S. Muntean, N. Pasca, L. Marsavina, Failure assessment of the shaft of a pumped storage unit, *Fatig. Fract. Eng. Mater. Struct.* 37 (7) (2014) 807–820, <https://doi.org/10.1111/ffe.12187>.
- [8] N.V. Kuznetsov, M.V. Yuldashev, R.V. Yuldashev, Analytical-numerical analysis of closed-form dynamic model of Sayano-Shushenskaya hydropower plant: stability, oscillations, and accident, *Commun. Nonlinear Sci. Numer. Simul.* 93 (2021), 105530, <https://doi.org/10.1016/j.cnsns.2020.105530>.
- [9] H. Li, D. Chen, E. Arzaghi, R. Abbassi, A. Kilicman, T. Caraballo, E. Patelli, X. Gao, B. Xu, Dynamic safety assessment of a nonlinear pumped-storage generating system in a transient process, *Commun. Nonlinear Sci. Numer. Simul.* 67 (2019) 192–202, <https://doi.org/10.1016/j.cnsns.2018.07.025>.
- [10] Z. Shen, X. Huang, Control of the turbine is operated side-by-side with the grid through long transmission lines, *J. Hydroelectr. Eng.* 26 (3) (1989) 77–86 (in Chinese)CNKI:SUN:SFXB.0.1989-03-008.
- [11] I.W. Group, Hydraulic turbine and turbine control model for system dynamic studies, *IEEE Trans. Power Syst.* 7 (1) (1992) 167–179, <https://doi.org/10.1109/59.141700>.
- [12] E.D. Jaeger, N. Janssens, Hydro turbine model for system dynamic studies, *IEEE Trans. Power Syst.* 9 (4) (1994) 1709–1715, <https://doi.org/10.1109/59.331421>.
- [13] Y. Cheng, L. Ye, Y. Liu, C. Fu, Z. Li, Design and implementation of a microcontroller-based governor for hydro turbine and its intelligent control strategy, *Int. J. Power Energy Syst.* 22 (3) (2002) 136–141.
- [14] K. Zhou, L. Zhang, Effects of weakly compressibility on propagating properties of water hammer in a long pipe, *Appl. Mech. Mater.* 444–445 (2013) 490–497, <https://doi.org/10.4028/www.scientific.net/AMM.444-445.490>.
- [15] W. Zeng, J. Yang, R. Tang, W. Yang, Extreme water-hammer pressure during one-after-another load shedding in pumped-storage stations, *Renew. Energy* 99 (2016) 35–44, <https://doi.org/10.1016/j.renene.2016.06.030>.
- [16] H. Bao, J. Yang, G. Zhao, W. Zeng, Y. Liu, Condition of setting surge tanks in hydropower plants - a review, *Renew. Sust. Energ. Rev.* 81 (2) (2018) 2059–2070, <https://doi.org/10.1016/j.rser.2017.06.012>.
- [17] Y. Liu, W. Guo, Coupling dynamic characteristics and transient power angle instability of grid-connected hydropower station with surge tank, *Int. J. Electr. Power Energy Syst.* 139 (2022), 107984, <https://doi.org/10.1016/j.ijepes.2022.107984>.
- [18] H. Li, D. Chen, H. Zhang, C. Wu, X. Wang, Hamiltonian analysis of a hydro-energy generation system in the transient of sudden load increasing, *Appl. Energy* 185 (2017) 244–253, <https://doi.org/10.1016/j.apenergy.2016.10.080>.
- [19] B. Xu, D. Chen, E. Patelli, H. Shen, J. Park, Mathematical model and parametric uncertainty analysis of a hydraulic generating system, *Renew. Energy* 136 (2019) 1217–1230, <https://doi.org/10.1016/j.renene.2018.09.095>.
- [20] B. Xu, D. Chen, X. Zhang, A. Riasi, Parametric uncertainty in affecting transient characteristics of multi-parallel hydropower systems in the successive load rejection, *Int. J. Electr. Power Energy Syst.* 106 (2019) 444–454, <https://doi.org/10.1016/j.ijepes.2018.10.029>.
- [21] J. Hou, C. Li, W. Guo, W. Fu, Optimal successive start-up strategy of two hydraulic coupling pumped storage units based on multi-objective control, *Int. J. Elec. Power.* 111 (2019) 398–410, <https://doi.org/10.1016/j.ijepes.2019.04.033>.
- [22] L. Lei, F. Li, K. Kheav, W. Jiang, X. Luo, E. Patelli, B. Xu, D. Chen, A start-up optimization strategy of a hydroelectric generating system: From a symmetrical structure to asymmetric structure on diversion pipes, *Renew. Energy* 180 (2021) 1148–1165, <https://doi.org/10.1016/j.renene.2021.09.010>.
- [23] P. Wang, D. Chen, H. Li, Hamiltonian modeling and energy analysis of a hydro electric generating set in the sudden load decreasing transient, in: Fluids Engineering Division Summer Meeting, American Society of Mechanical Engineers. Virtual, Online, July 13–15 83723, 2020, <https://doi.org/10.1115/FEDSM2020-20113>. V002T03A002.
- [24] Y. Zeng, L. Zhang, Y. Guo, J. Qian, C. Zhang, The generalized Hamiltonian model for the shafting transient analysis of the hydro turbine generating sets, *Nonlinear Dyn* 76 (4) (2014) 1921–1933, <https://doi.org/10.1007/s11071-014-1257-9>.
- [25] B. Guo, B. Xu, D. Chen, W. Ye, H. Li, Vibration characteristics of the hydroelectric generating systems during load rejection transient process, *J. Comput. Nonlin. Dyn.* 14 (2019), 071006, <https://doi.org/10.1115/1.4043361>.
- [26] H. Li, D. Chen, B. Xu, S. Tolo, E. Patelli, Dynamic analysis of multi-unit hydropower systems in transient process, *Nonlinear Dyn.* 90 (1) (2017) 535–548, <https://doi.org/10.1007/s11071-017-3679-7>.
- [27] Y. Guo, X. Liang, Z. Niu, Z. Cao, L. Lei, H. Xiong, D. Chen, Vibration characteristics of a hydroelectric generating system with different hydraulic-mechanical-electric parameters in a sudden load increasing process, *Energies* 14 (21) (2021) 7319, <https://doi.org/10.3390/en14217319>.
- [28] J. Zhou, X. Peng, R. Li, Y. Xu, D. Chen, Experimental and finite element analysis to investigate the vibration of oblique-stud stator frame in a large hydropower generator unit, *Energies* 10 (12) (2017) 2175, <https://doi.org/10.3390/en10122175>.
- [29] Q. Wu, L. Zhang, Z. Ma, A model establishment and numerical simulation of dynamic coupled hydraulic-mechanical-electric-structural system for hydropower station, *Nonlinear Dyn.* 87 (1) (2017) 459–474, <https://doi.org/10.1007/s11071-017-16.001>.
- [30] L. Zhang, Q. Wu, Z. Ma, X. Wang, Transient vibration analysis of unit-plant structure for hydropower station in sudden load increasing process, *Mech. Syst. Signal Proc.* 120 (2019) 486–504, <https://doi.org/10.1016/j.ymssp.2018.10.037>.
- [31] S. Wan, Y. He, Investigation on stator and rotor vibration characteristics of turbo-generator under air gap eccentricity fault, *Trans. Canad. Soc. Mech. Eng.* 35 (2) (2011) 161–176, <https://doi.org/10.1139/tcsme-2011-0010>.
- [32] Y. Li, G. Zhou, S. Wan, H. Li, Analysis of unbalanced magnetic pull on turbo-generator rotor under air-gap eccentric fault and rotor short circuit fault, *Int. J. Adv. Comput. Technol.* 5 (4) (2013) 523–530, <https://doi.org/10.4156/ijact.vol5.issue4.62>.
- [33] Y. Callecharan, R. Jauregui, J.O. Aidanp, Towards a general method for estimating the unbalanced magnetic pull in mixed eccentricities motion including sufficiently large eccentricities in a hydropower generator and their validation against em simulations, *Eur. Phys. J. Appl. Phys.* 63 (2) (2016) 20901, <https://doi.org/10.1051/epjap/2013130092>.
- [34] Q. Wu, L. Zhang, Z. Ma, Expansion and reconstruction of comprehensive characteristic curve for water turbine based on engineering experience and RBF neural network, *J. Basic Sci. Eng.* 27 (5) (2019) 996–1007 (in Chinese)CNKI:sun:yjgx.0.2019-05-005.
- [35] W. Sun, Z. Guo, Mathematical modeling and nonlinear vibration analysis of a coupled hydro-generator shaft-foundation system, *Commun. Nonlinear Sci. Numer. Simul.* 98 (2021), 105776, <https://doi.org/10.1016/j.cnsns.2021.105776>.
- [36] J. Zhang, L. Zhang, Z. Ma, X. Wang, Q. Wu, Z. Fan, Coupled bending-torsional vibration analysis for rotor-bearing system with rub-impact of hydraulic generating set under both dynamic and static eccentric electromagnetic excitation, *Chaos Soliton Fract.* 147 (2021), 110960, <https://doi.org/10.1016/j.chaos.2021.110960>.
- [37] L. Zhang, Z. Ma, Q. Wu, X. Wang, Vibration analysis of coupled bending-torsional rotor-bearing system for hydraulic generating set with rub-impact under electromagnetic excitation, *Arch. Appl. Mech.* 86 (9) (2016) 1665–1679, <https://doi.org/10.1007/s00419-016-1142-8>.

- [38] H. Bao, J. Yang, F. Liang, Study on nonlinear dynamical model and control strategy of transient process in hydropower station with Francis turbine, in: Asia-Pacific Power and Energy Engineering Conference, IEEE, Wuhan, China, March 27–31, 2009, pp. 1–6, <https://doi.org/10.1109/APPEEC.2009.4918827>.
- [39] Y. Xu, Y. Zheng, Y. Du, W. Yang, X. Peng, C. Li, Adaptive condition predictive-fuzzy pid optimal control of start-up process for pumped storage unit at low head area, *Energy Conv. Manag.* 177 (2018) 592–604, <https://doi.org/10.1016/j.enconman.2018.10.004>.
- [40] B. Xu, F. Wang, D. Chen, H. Zhang, Hamiltonian modeling of multi-hydro-turbine governing systems with sharing common penstock and dynamic analyses under shock load, *Energy Conv. Manag.* 108 (2016) 478–487, <https://doi.org/10.1016/j.enconman.2015.11.032>.